HHS Public Access

Author manuscript

Neuron. Author manuscript; available in PMC 2024 October 18.

Published in final edited form as:

Neuron. 2023 October 18; 111(20): 3244–3254.e8. doi:10.1016/j.neuron.2023.07.010.

A novel immune modulator IM33 mediates a glia-gut-neuronal axis that controls lifespan

Wangchao Xu[1,2,*], **Justin Rustenhoven**[1,2,3,4], **Christopher A. Nelson**[2], **Taitea Dykstra**[1,2], **Aura Ferreiro**[5,6], **Zachary Papadopoulos**[1,2,7], **Carey-Ann D. Burnham**[2], **Gautam Dantas**[2,5,6,8], **Daved H. Fremont**[2,8,9,10], **Jonathan Kipnis**[1,2,7,*]

[1]Brain Immunology and Glia (BIG) Center, Washington University in St. Louis, School of Medicine; St. Louis, MO, USA

[2]Department of Pathology and Immunology, Washington University in St. Louis, School of Medicine; St. Louis, MO, USA

[3]Department of Pharmacology and Clinical Pharmacology, The University of Auckland, Auckland, New Zealand

[4]Centre for Brain Research, The University of Auckland, Auckland, New Zealand

[5]The Edison Family Center for Genome Sciences and Systems Biology, Washington University in St. Louis, School of Medicine; St. Louis, MO, USA

[6]Department of Biomedical Engineering, Washington University in St. Louis; St. Louis, MO, USA

[7]Neuroscience Graduate Program, School of Medicine, Washington University in St. Louis, School of Medicine; St. Louis, MO, US.

[8]Department of Molecular Microbiology, Washington University in St. Louis, School of Medicine; St. Louis, MO, USA

[9]The Andrew M. and Jane M. Bursky Center for Human Immunology and Immunotherapy Programs, Washington University School of Medicine; St Louis, MO, USA

[10]Department of Biochemistry & Molecular Biophysics, Washington University School of Medicine; St Louis, MO, USA

[*]Correspondence: W.X. (xu.w@wustl.edu) or J.K. (kipnis@wustl.edu); Tel: 001 314-273-2288 Lead Contacts: Jonathan Kipnis (kipnis@wustl.edu).

Author contributions

W.X. designed and performed all the *Drosophila*-related experiments, analyzed and interpreted the data, created the figures and wrote the manuscript. J.R. performed the mouse experiments, analyzed the data, helped with cell sorting and scRNA sequencing and participated in methods writing; C.N. purified the IM33 protein and participated in methods writing; T.D. performed the scRNAseq data analysis and participated in methods writing; A.F. performed the 16S rRNA seq data analysis and participated in methods writing; Z.P. wrote the codes for sleep data analysis; C.D.B. helped with the bacteria culture and isolation; G.D. supervised the 16S rRNA seq data analysis; D.F. supervised the IM33 protein purification; J.K. designed the experiments, provided intellectual contributions, analyzed and interpreted the data and wrote the manuscript.

Declaration of interests

The authors declare no competing interests.

Summary

Aging is a complex process involving various systems and behavioral changes. Altered immune regulation, dysbiosis, oxidative stress, and sleep decline are common features of aging, but their interconnection is poorly understood. Using *Drosophila*, we discover that IM33, a novel immune modulator, and its mammalian homolog, SLPI, are upregulated in old flies and old mice, respectively. Knockdown of IM33 in glia elevates the gut reactive oxygen species (ROS) level and alters gut microbiota composition, including increased *Lactiplantibacillus plantarum* abundance, leading to a shortened lifespan. Additionally, dysbiosis induces sleep fragmentation through the activation of insulin-producing cells in the brain, which is mediated by the binding of *Lactiplantibacillus plantarum*-produced DAP-type peptidoglycan to the peptidoglycan recognition protein LE (PGRP-LE) receptor. Therefore, IM33 plays a role in the glia-microbiota-neuronal axis, connecting neuroinflammation, dysbiosis and sleep decline during aging. Identifying molecular mediators of these processes could lead to the development of innovative strategies for extending lifespan.

eTOC blurb

Xu et al. used *Drosophila* to identify a novel immune modulator that mediates a brain-gut-brain axis, connecting four aspects of aging: neuroinflammation, dysbiosis, oxidative stress, and sleep decline.

Graphical Abstract

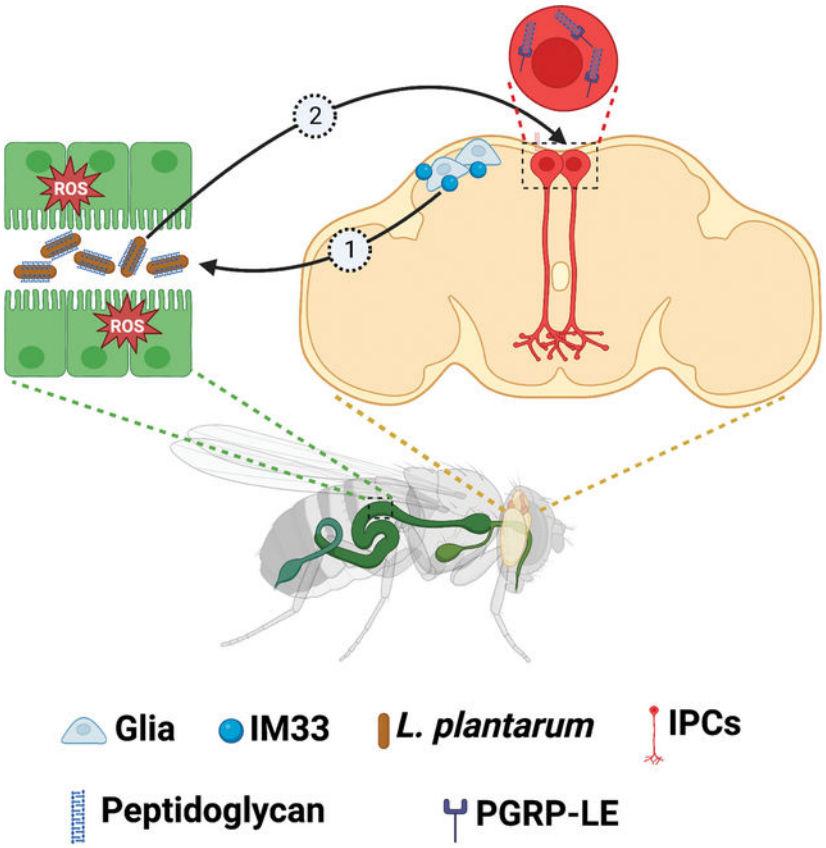

Introduction

Aging takes its toll on virtually every tissue in the body [1]. The immune system is itself not immune to aging-associated loss of function, and its adaptive arm is arguably the one most affected during aging [2]. To compensate for immune dysfunction, the body may default to more primitive immune mechanisms such as producing antimicrobial peptides and other immune molecules [3,4]. These molecules are highly expressed in the brain and its borders, raising an interesting question as to their function under physiological conditions[5,6]: for instance, could they serve as messengers conveying information between tissues?

Dysbiosis has emerged as a hallmark of aging [7], and maintaining gut microbiota homeostasis is crucial for healthy aging [8]. As aging-induced inflammation is one of the major contributors to dysbiosis [8], a precise immunomodulation involving the nevous system is required to control inflammation and stabilize microbiota [9]. While the central nervous system has been identified as the regulatory center of the inflammatory reflex [9], its impact on microbiota in aging remains unclear. Alongside dysbiosis, oxidative stress is another component of the aging gut [8]. Accumulation of reactive oxygen species (ROS) in the gut has been shown to be the cause of premature mortality resulting from sleep loss [10], underscoring the importance of gut ROS for survival. However, the relationship between the aging brain and gut ROS is poorly understood.

Given the well-established gut-brain axis [11–13], dysbiosis can affect brain function and lead to behavioral alterations. A decline in sleep quality is a common manifestation of aging [14–16], yet the extent to which it is influenced by microbiome imbalance remains largely unknown.

Here, using *Drosophila* as a tractable model to study the innate immune regulation of aging, we identified a glia-derived immune modulator, IM33, as a key molecule to maintain gut homeostasis and sustain a normal lifespan. Furthermore, loss of function of IM33 in glia results in a daytime sleep impairment through a glia-microbiota-neuronal axis.

Results

Glia-derived IM33 is required to sustain the lifespan

To screen for the immune products from *Drosophila* that are conserved, we used protein sequence alignment and identified immune induced molecule 33 (IM33) as the only immune product having mammalian homologs, namely epididymal peptidase inhibitor (EPPIN) and secretory leukocyte protease inhibitor (SLPI) (FlyBase.org) (Fig. S1A), both of which have antimicrobial functions. Despite the low amino acid identity between IM33 and EEPIN or SLPI, they shared the bovine pancreatic trypsin inhibitor domain. Interestingly, single-cell RNA sequencing of the brain and meningeal stroma from young and old mice[17] indicated that Slpi is strongly induced in the meninges (triple-layered membranes surrounding the brain) of old mice (Fig. S1B). We confirmed this using ELISA, and also observed upregulation of SLPI in the large intestine and skin of old mice (Fig. S1C). These data suggest that aging-induced SLPI is selective for barrier tissues, including the dura, which is the border of the brain. We also found IM33 mRNA induction in old flies, which was more substantial in the head than in the body (Fig. 1A, Fig. S1D).

To investigate the function of IM33 in aging, we measured the lifespan of flies with neuron-specific or glia-specific knockdown of IM33 and found that only the latter exhibited reduced longevity (Fig. 1B, C). This reduction was not due to developmental deficits, as knocking down IM33 in glia from adulthood using a glia-specific GeneSwitch system [18,19] resembled the shortened lifespan (Fig. 1D). We validated these findings using another line with slightly less RNA interference (RNAi) efficiency and another RNAi control line in male but not in female flies (Fig. S1E–G). Since fat body and hemocytes are the main immune tissues in flies, we tested whether the IM33 deficiency in these cells also affected lifespan. In contrast to glia, knockdown of IM33 in fat body or hemocytes slightly extended the lifespan (Fig. S1H, I). Moreover, global knockout of IM33 showed a lifespan similar to that of control flies (Fig. S1J), suggesting a unique mechanism by which glia-derived IM33 controls lifespan. As the glial knockdown of IM33 caused a pronounced lifespan reduction, our study mainly focused on glia-derived IM33.

To evaluate the sufficiency of IM33, we overexpressed it in glia either from the developmental stage or in adulthood. We observed an extension of lifespan (Fig. 1E, Fig. S1K, L) as well as a rescue of aging-induced motor disability (Fig. 1F), suggesting that IM33 plays a role in controlling the lifespan.

To determine whether these effects were dependent on the secretion of IM33, we expressed an HA-tagged IM33 lacking the secretion peptide (1–19 aa) (IM33$^{\Delta SP}$-HA) in glia. In contrast to the HA-tagged full-length IM33 (IM33-HA), which is enriched at the brain border (Fig. S1M), deletion of the signal peptide retains IM33 in glial cell bodies (Fig. S1N). Moreover, a secretion-deficient mutant failed to prolong the lifespan (Fig. S1O, P), suggesting the effect of IM33 on lifespan is secretion-dependent.

To visualize IM33 expression in glia, we generated an IM33-Gal4 line that drove the expression of nuclear-localized RFP (RedStinger). We observed that RFP-positive cells were sparsely distributed at the border and surface of the brain (Fig. 1G). Some of these cells were also colocalized with the glial marker Repo (Fig. 1H, Fig. S1Q, R). A similar pattern was also observed in IM33-GFP knock-in flies (Fig. S1S, T), although the signal of endogenous IM33 was faint due to its low expression level and active secretion. The expression pattern of IM33 is reminiscent of the high SLPI expression observed in old mouse meninges rather than the brain parenchyma.

IM33 is a novel immune modulator that shapes the gut microbiota

As reported[20], IM33 was upregulated upon *E. coli* infection (Fig. S2A), but the induction was not as strong as Diptericin A, a well-characterized anti-Gram negative antimicrobial peptide (AMP) (Fig. S2B). To investigate whether IM33 has an antimicrobial function, we infected IM33 knockout flies with *E. coli* and observed an increase in *E. coli* load in these flies (Fig. 2A). However, incubation of the purified IM33 protein with *E. coli* failed to suppress the growth of bacteria (Fig. S2C), suggesting that the impact of IM33 on *E. coli* infection *in vivo* is indirect. This was confirmed by the blunted induction of anti-Gram negative AMPs upon *E. coli* challenge in the IM33 knockout flies (Fig. 2B), indicating that IM33 regulates the expression of AMPs but does not have its own antimicrobial activity.

As the gut AMPs are tightly controlled and could be regulated by the brain-gut axis[12], we asked whether the glia-derived IM33 is required to maintain the gut microbiota homeostasis. Accompanied by the decreased expression of several AMPs in the gut of flies with glial IM33 knockdown (Fig. 2C), the amount of Lactobacillus was increased, leading to an altered microbiota composition and recapitulating the aging effects on microbiota (Fig. 2D, E, Fig. S2D). In contrast to IM33 knockdown, overexpression of IM33 in glia reduced Lactobacillus in a secretion-dependent fashion (Fig. S2E). Overall, our results suggest that IM33 could function as an immune regulator in both homeostasis and infection.

A deep analysis of the 16s-sequencing dataset revealed *Lactiplantibacillus plantarum* (*L. plantarum*) as the predominant Lactobacillus species enriched in IM33 RNAi flies (Fig. S2F), which was verified by qPCR using *L. plantarum*-specific primers [21] (Fig. 2F, Fig. S2G), whereas IM33 overexpression in glia reduced the abundance of *L. plantarum* (Fig. S2H). To determine whether the enrichment of *L. plantarum* causes the shotenend lifespan, we transferred *L. plantarum* to germ-free flies and assessed the lifespan. Consistent with the previous study [22,23], colonization of *L. plantarum* significantly decreased the lifespan (Fig. 2G). In contrast, monoassociation with *Lactobacillus brevis* (*L. brevis*), another common Lactobacillus in fly gut, showed no effects on lifespan (Fig. 2G).

The expression of IM33 in the gut is exclusive to the foregut and hindgut (Fig. S2I, J), and this pattern remains consistent during aging (Fig. S2K). While the mRNA of gut IM33 increased in old flies (Fig. S2L), knockdown of IM33 in intestinal stem cells or enterocytes showed no effects on lifespan (Fig. S2M, N). Furthermore, no leaky expression of Repo-Gal4 in the gut was detected by using either GFP reporters or quantitative real-time PCR (Fig. S2O–Q). This further supports the notion that the microbiota is shaped by IM33 secreted from glia. On the other hand, IM33 induction by aging is microbiota-dependent because depletion of the microbiota by an ampicillin/doxycycline/kanamycin antibiotic cocktail (ABX) prevented the upregulation of IM33 in old flies (Fig. S2R), suggesting a reciprocal regulation between gut microbiota and brain IM33.

Loss of IM33 in glia causes an accumulation of ROS in the gut

The impact on longevity resulting from *L. plantarum* colonization was less pronounced compared to the effects of IM33 knockdown, indicating the involvement of another mechanism. Dysbiosis is closely associated with overproduction of reactive oxygen species (ROS), a known factor contributing to shortened lifespan [24]. To test whether IM33 knockdown in glia increases the level of ROS, we used Dihydroethidium (DHE) as the probe to detect ROS in living tissues [10]. Elevated ROS level was observed in the gut but not the brain of the flies with glial IM33 knockdown (Fig. 2H, I, Fig. S2S, T). Moreover, feeding the flies with lipoic acid [10], a ROS scavenger, significantly reduced the ROS level and partially rescued the shortened lifespan (Fig. 2H–J). These findings suggest that ROS accumulation in the gut mediates the mechanism through which glia-derived IM33 regulates lifespan.

Glia-microbiota axis in sleep regulation

Since the gut-brain communication is well-established [11,12,13,25], we wondered whether the gut dysfunction alters brain functions. We assessed brain morphology, metabolisms and various behaviors, and only observed sleep deficits in flies with IM33 knockdown in glia. Specifically, knockdown of IM33 in glia, but not in neurons, led to fragmentation of daytime sleep in young flies, as indicated by a decrease in sleep bout length and an increase in sleep bout number (Fig. 3A–D, Fig. S3A–D). The sleep phenotype was also observed when IM33 RNAi was started in adulthood (Fig. S3E). Spontaneous locomotion, circadian rhythm, food intake, brain cell survival, glucose and triglyceride level were not affected (Fig. S3F–O).

To understand the relationship between daytime sleep deficits and reduced longevity, we simulated daytime sleep fragmentation using a mechanical shaker (Fig. S4A–B) and found a significant but slight decrease in the lifespan (Fig. S4C), indicating that sleep deficits is not the primary driver for aging. However, treatment with THIP (also known as Gaboxadol), a sleep-promoting compound [26] improved daytime sleep (Fig. 3A–D) and largely restored the lifespan without affecting the immune functions, microbiota or food consumption in young flies with glial IM33 knockdown (Fig. 3E, Fig. S4D–G). Notably, THIP treatment in wild-type flies showed no impact on lifespan (Fig. S4H). Inducing daytime sleep fragmentation weakened the beneficial effect of THIP on lifespan (Fig. 3E), suggesting that THIP-mediated daytime sleep improvement partially prevented the early aging of glial IM33-deficient flies. It is worth noting that long-term activation of GABAergic neurons

can have broader effects, and we cannot exclude the possibility that lifelong treatment with THIP rescues the shortened lifespan through other mechanisms. We attempted to thermogenetically improve daytime sleep by activating dorsal fan-shaped body neurons as an alternative approach [27] (Fig. S4I), but this failed to extend the lifespan of flies with glial IM33 deficiency (Fig. S4J), mainly due to the masking effect of high-temperature treatment on lifespan. It has been reported that ROS accumulation in the gut mediated the early death caused by long-term sleep deprivation [10,28], leading us to question whether the increased amount of ROS was a consequence of sleep fragmentation. High ROS persisted in the flies with THIP treatment, indicating that the ROS accumulation is not caused by abnormal daytime sleep (Fig. 2I). Feeding with a combination of lipoic acid and THIP completely rescued the shortened lifespan (Fig. S4K), suggesting that the benefical effects of THIP are independent of ROS. In contrast to IM33 RNAi, overexpression of the full-length IM33-HA but not IM33$^{\Delta SP}$-HA (secretion deficient protein) in glia improved both daytime and nighttime sleep (Fig. S4L–N).

Next we tested whether sleep impairment was caused by dysbiosis. Microbiota depletion with antibiotic treatment (ABX) completely rescued the daytime sleep fragmentation in flies with glial IM33 knockdown (Fig. 3F). Consistently, using germ-free flies to eliminate the microbiota from the embryonic stage also restored the daytime sleep bout number (Fig. S4O). Moreover, the sleep improvement achieved upon IM33 overexpression was abolished by ABX treatment (Fig. S4P, Q). These changes are not due to brain toxicity from ABX treatment, as we found no increase in cell death or damage markers (Fig. S5R, S). Together, these data demonstrate that the modulation of sleep by glial IM33 is microbiota-dependent.

L. plantarum is the culprit of the sleep defect

Since the accumulation of *L. plantarum* contributed to the shortened lifespan (Fig. 2F, G), we investigated whether *L. plantarum* is also the root cause of defective daytime sleep observed in these flies. Transfer of *L. plantarum* to ABX-treated flies resulted in the induction of IM33 in the head but not in the gut (Fig. S5A, B). On the contrary, *L. plantarum* transfer to flies with intact microbiota failed to upregulate the expression of IM33 (Fig. S5C). The efficiency of *L. plantarum* colonization was determined by qPCR (Fig. S5D). Sleep assays indicated that monoassociation of *L. plantarum* in ABX-treated or germ-free flies phenocopied the daytime sleep fragmentation (Fig. 4A, B, Fig. S5E, F), whereas *L. brevis*, which is responsible for the modulation of locomotion [29], showed no effect on sleep despite the induction of IM33 by *L. brevis* transfer (Fig. 4A, B, Fig. S5G), arguing that sleep regulation is *L. plantarum* specific. The glucose and triglyceride levels are not altered by *L. plantarum* transfer (Fig. S5H, I). To understand why daytime sleep was selectively perturbed, we assessed the amount of *L. plantarum* in flies with glial IM33 RNAi at different time points over a 24-hour period and found that the level of gut *L. plantarum* lowered at ZT8 and peaked at ZT20 (Fig. 4C). The oscillation of *L. plantarum* is a potential mechanism of the selective disturbance of daytime sleep. Taken together, these findings demonstrate that the accumulation of *L. plantarum* in the gut was the cause of daytime sleep fragmentation.

Microbiota-neuronal axis in sleep regulation

To understand how *L. plantarum* modulates sleep behavior, we performed single-cell RNA sequencing of fly brains from three age-matched groups: untreated flies (CTRL), antibiotic-treated flies (ABX) and *L. plantarum*-transferred flies (LP). Consistent with a previous report[30], all the major cell types in the fly brain were identified in our dataset (Fig. 5A). In all clusters, cells from the 3 groups were evenly distributed and intermingled (Fig. 5B). However, gene ontology analysis of cholinergic neurons revealed an overrepresentation of sleep and circadian pathways in the downregulated genes from the comparison of LP with ABX (Fig. S6A, Tables S1, S2). Moreover, several sleep-related genes[31] were also differentially expressed (Fig. 5C). The increase in insulin-like peptide 2 (Ilp2) and insulin-like peptide 5 (Ilp5) after *L. plantarum* transfer led us to hypothesize that insulin-producing cells (IPCs) are the downstream target of *L. plantarum*, since IPCs serve both as sensors to peripheral signals and as sleep regulators [32]. Using ILP2-Gal4 to express CaLexA, whose GFP intensity reflects the strength of sustained neuronal activation[33], we observed an increase in the CaLexA signal in IPCs four days after *L. plantarum* transfer, compared to untreated, ABX-treated or *L. brevis*-transferred flies (Fig. 5D, E). Interestingly, the increased activity of IPCs upon *L. plantarum* transfer was not detected at night (ZT16) (Fig. S6B), attributing to an increase in the baseline activity. The differential day-and-night activity of IPCs might be the mechanism of selective impairment of daytime sleep. *L. plantarum* transfer to the flies with intact microbiome was not able to activate the IPCs (Fig. S6C) due to a failure of colonization (Fig. S5D). Moreover, Dh44 neurons, another type of nutrient-sensing neuron located in the same brain region with IPCs, or the other types of neurons, did not respond to *L. plantarum* (Fig. S6D), suggesting that activation by *L. plantarum* is selective to IPCs.

To examine whether IPCs mediate *L. plantarum* modulation of sleep, we expressed a temperature-sensitive shibire mutant[34] in IPCs to manipulate neuronal activity. Compared with ABX treatment, *L. plantarum* colonization caused daytime sleep fragmentation when the synaptic function of IPCs was preserved (18°C). However, subsequent switching to 29°C, which blocks the synaptic transmission, eliminated the differences in daytime sleep bout length and number between ABX treatment and *L. plantarum* transfer (Fig. 5F, Fig. S6E). This was not caused by the impact of the temperature shift itself, because the sleep phenotype persisted in control (ILP2/+) flies (Fig. S6F). These findings demonstrate that neural activity of IPCs mediates the effects of *L. plantarum* on sleep and establish a microbiota-neuronal axis for sleep regulation.

Peptidoglycan-PGRP-LE signaling in sleep regulation

To find what metabolites derived from *L. plantarum* mediate sleep regulation, we compared *L. plantarum* and *L. brevis* and found that one of the major differences was the type of peptidoglycans (*L. plantarum*: DAP-type; *L. brevis*: Lys-type)[35]. Since peptidoglycan was recently shown to be a new regulator of brain function [36,37], we tested whether DAP-type peptidoglycan (PG) is able to mimic *L. plantarum* effects. Feeding the flies with DAP-type PG was sufficient to induce activation of IPCs and daytime sleep fragmentation (Fig. 6A–C). Furthermore, *ex vivo* calcium imaging also showed that the application of DAP-type PG but

not the recombinant IM33 protein to the brain increased the calcium influx in IPCs (Fig. 6D–F, Fig. S6G, H, Movie S1), suggesting a direct action of DAP-type PG on IPCs.

To search for the receptor responsible for the DAP-type PG-mediated sleep modulation, we used an RNAi strategy to screen for all the potential receptors of DAP-type PG and identified peptidoglycan recognition protein LE (PGRP-LE) as the major responder, because knockdown of PGRP-LE in IPCs completely prevented the daytime sleep fragmentation caused by *L. plantarum* transfer or PG treatment (Fig. 6G, H). The shortened lifespan caused by *L. plantarum* transfer was rescued as well by PGRP-LE knockdown (Fig. 6I). Moreover, knockdown of PGRP-LE in IPCs alone is sufficient to extend the lifespan (Fig. 6J), revealing a potential new target to combat aging. Collectively, our results demonstrate that the *L. plantarum*-derived PG signals on the PGRP-LE in IPCs to cause the sleep phenotype.

Discussion

In this study, we identified glia-derived IM33, an immune modulator that connects four aspects of aging: aberrant immunity, dysbiosis, ROS accumulation and sleep decline. In contrast to AMPs, IM33 has a positive effect on aging, as its overexpression promotes healthy aging and extends lifespan, while the overproduction of most AMPs leads to neurodegeneration [38,39]. The upregulation of classical AMPs is an inflammatory response to aging and is detrimental to lifespan. However, the induction of brain IM33 is a compensatory response to aging-induced dysbiosis, making IM33 distinct from other immune molecules.

The opposing effects on the lifespan of IM33 derived from glia versus peripheral tissues suggest that glia-secreted IM33 utilizes a distinct mechanism to regulate the brain-gut axis. Since IM33 is expressed in a limited number of glia, its immune modulatory effects may need to be amplified. This amplification could potentially occur through the neurons that innervate or remotely control the gut. Previous studies have shown that AMPs can bind to neuropeptide receptors and induce sleep in *C. elegans* [40], but it remains to be determined if this mechanism is also involved in flies and warrants further investigation.

IM33 sustains the lifespan by controlling the gut microbiota and ROS level. Dual oxidase, an NADPH oxidase enzyme that is essential for ROS generation, has been identified as a key player in the control of gut microbiota [41]. The metabolites derived from gut microbes, in turn, have been implicated in regulating ROS production [24]. Therefore, dysbiosis and oxidative stress can form a vicious cycle that drives the acceleration of aging.

The cause of the selective disruption of daytime sleep in flies with glial IM33 knockdown is still a mystery. We speculate that the oscillation of *L. plantarum* level may contribute to the difference in the day-night activity of IPCs. It has been reported that the microbiota did not cycle in the wild-type flies fed *ad libitum* [42], making it intriguing how the loss of glial IM33 leads to a circadian fluctuation of *L. plantarum*. Since microbiota and circadian rhythms are reciprocally regulated [43], it is possible that the glia-derived IM33 act on circadian pacemaker neurons to regulate the microbiota oscillation.

Accumulating evidence points to an important role of microbiota in the regulation of brain functions [12,13,25]. *L. brevis* and *Acetobacter pomorum* participate in the modulation of host locomotion and in sensing essential amino acids, respectively [29,44]. Here we introduce *L. plantarum* as a regulator of the quality of daytime sleep. These findings inspire us to propose that various combinations of gut commensal bacteria may serve as specific modulators of certain behaviors. Given the simplicity of the fly microbiome, it will be feasible to conduct a systematic assessment of behaviors using gnotobiotic flies. In contrast to our findings, certain strains of *L. plantarum* have been reported to have probiotic effects in vertebrates [45,46], indicating that the variability and complexity of the microbiota play a role in determining the outcomes across different species. By examining the impact of a particular commensal bacteria on various organisms, we can gain a better understanding of how the microbiota-gut-brain axis is influenced by evolution.

Peptidoglycan was recently discovered to be a novel metabolite that regulates neurodevelopments and behaviors [37,47]. Our findings indicate that peptidoglycan plays a conserved role in neuronal function throughout evolution, and that genetically blocking the peptidoglycan receptor can extend lifespan. A deeper understanding of peptidoglycan signaling in the brain may foreshadow the development of therapeutic interventions for the modulation of complex behavioral disorders and slowing down the aging process.

STAR methods

Resource availability

Lead contact—Further information and requests for resources and reagents should be directed to and will be fulfilled by the lead contact, Jonathan Kipnis (kipnis@wustl.edu).

Materials availability—The new *Drosophila* lines generated here are available upon request to the lead contact.

Data and code availability—16S sequencing and single-cell RNA-seq data have been deposited at GEO and are publicly available as of the date of publication. Accession numbers are listed in the key resources table. Microscopy data reported in this paper will be shared by the lead contact upon request.

The original code is available upon request to the lead contact.

Any additional information required to reanalyze the data reported in this paper is available from the lead contact upon request.

Experimental Model and Study Participant Details

Mice—Mice were housed under pathogen-free, temperature and humidity-controlled conditions with a 12-hour light cycle. Mice were housed no more than 5 animals in a cage with rodent chow and water provided *ad libitum*. In all experiments, male mice were used. Adult mice (8–12 weeks old) used in this study were C57BL/6J purchased from Jackson Laboratory (WT; JAX000664). Aged mice (20–24 months) were obtained from the National Institutes of Aging. All experiments were approved by the Institutional Animal

Care and Use Committee of the University of Virginia and/or Washington University in St. Louis. Experiments were only performed in institutions for which experimental approval was granted.

Drosophila: Flies were kept on standard fly food which is purchased from LabExpress (7001-PNV). Unless stated otherwise, all flies were maintained at the incubator with the temperature set at 24°C, humidity set at 60% and 12 h light/dark cycle. Isogenic w^{1118} (BDSC #5905) was used as wild-type (WT) flies. Male flies were used in all the experiments unless otherwise indicated. Except for the Glia-GeneSwitch, UAS-shibire and PGRP RNAi screening experiments, all the flies were backcrossed with wild-type for 8 generations before experiments. Unless indicated in the figures or figure legends, flies aged 5–7 days were used for the experiments.

Method Detail

Protein isolation and ELISA—Adult (2–3 months) and aged (20–24 months) mice were given a lethal dose of i.p. Euthasol (10% v/v) and perfused via transcardial perfusion with 0.025% heparin in PBS. Skull caps were removed from the mice and cranial dura was peeled from the skull in sterile PBS. Peeled dura and other dissected tissues were transferred to tissue lysis buffer (100 mM Tris, pH 7.4, 150 mM NaCl, 1 mM EGTA, 1 mM EDTA, 1% Triton X-100, 0.5% Sodium deoxycholate, 1 mM PMSF and 1X Complete Mini ETA Protease inhibitor cocktail (Sigma Aldrich)). Samples were homogenized using a Mini Beadbeater (BioSpec Products) and 2.3-mm zirconia-silica beads (BioSpec Products). Protein concentrations were determined using a DC Protein assay (5000112, BioRad) as per manufacturer's instructions and concentrations equalized with tissue lysis buffer. SLPI concentrations were determined using the Mouse SLPI ELISA kit (LS-F6729-1, LifeSpan Biosciences) as per manufacturer's instructions using a spectrometer (Fisher Scientific).

Generation of IM33-Gal4 flies—2000 bp DNA sequence upstream of start codon of IM33 was amplified from fly genome by using IM33 Gal4-F and IM33 Gal4-R primers, and was cloned into pBPGw plasmid (#17574, addgene) using in-fusion cloning technology (638948, Takara Bio). The plasmids were injected into y[1] w[67c23]; P{y[+t7.7]=CaryP}attP1 (BDSC#8621) at BestGene Inc in accordance to the standard microinjection protocol.

Generation of the UAS lines—IM33, IM33-HA and IM33-HA without signal peptide were amplified using the following pairs of primer respectively: IM33 CDS-F and IM33 CDS-R, IM33 CDS-F and IM33 CDS-HA-R, IM33 CDS W/O SP-F and IM33 CDS-HA-R. The purified PCR products were cloned into pUAST (#1000, DGRC) using EcoRI and XhoI restrictive sites. The plasmids were injected into w^{1118} by BestGene Inc according to the standard microinjection protocol.

Generation of the IM33-GFP knock-in and IM33 knockout flies—We generated the IM33-GFP knock-in flies by following the published protocols[48]. First, using different primer pairs (IM33-R-F and IM33-R-R, IM33-GFP-L1-F and IM33-GFP-PAM L1-R, IM33-GFP-L3-F and IM33-L3-R) to amplify the 3' arm, fragment 1 and 3 of the 5' arm from

vas-Cas9 fly genome respectively. Second, amplify fragment 2 of 5' arm from pEGFP-C3 (#6082–1, addgene) plasmid using IM33-GFP-PAM L2-F and IM33-GFP-L2-R, followed by overlapping PCR to combine the 3 fragments together to obtain the 5' arm. Last, insert the 3' arm and 5' arm into pHD-ScarlessDsRed (#1364, DGRC) by SapI and AarI digestion respectively.

The IM33 knockout flies were generated by replacing the IM33 coding sequence with GFP. PCR product amplified from vas-Cas9 fly genome (IM33-L1-F and IM33 del-GFP-L1-R) and from IM33-GFP knock-in plasmid (IM33 del-GFP-L2-F and IM33-L3-R) were combined by overlapping PCR to make the 5' arm. Together with the 3' arm made above were inserted into pHD-ScarlessDsRed.

To make the gRNA construct, we conducted annealing using primer pairs of IM33-GFP-gRNA-F and IM33-GFP-gRNA-R for IM33-GFP knock-in, and primer pairs of IM33 del-GFP-gRNA-F and IM33 del-GFP-gRNA-R for IM33 knockout. The gRNA was then inserted into pU6-BbsI-gRNA (#1363, DGRC) with the restrictive enzyme BbsI.

The pHD-ScarlessDsRed and pU6-BbsI-gRNA vectors were mixed and injected into the vas-Cas9 by BestGene Inc. The flies with red fluorescent eyes were collected, and the successful transformants were confirmed by sequencing.

Generation of germ-free flies—Germ-free flies were generated by following the published method[49]. Briefly, parent flies were placed in a container covered with grape-juice agar plate overnight. Embryos were collected and rinsed in sterilized water with 0.6% sodium hypochlorite. Transfer the embryos to vials containing sterile fly food and grow them in the incubator.

GeneSwitch induction—200 μL of 1 mM RU486 (Mifepristone, M8046, Sigma-Aldrich) or vehicle (100% ethanol) was added to the surface of fly food in vials and allowed to dry overnight. Flies were transferred to fresh drug- or vehicle-treated food vials every 4 days.

To monitor the locomotion and sleep, RU486 was mixed with DAM food (5% sucrose and 2% Bacto agar (214010, BD)) at the final dosage of 1 mM.

Purification of IM33 protein—A synthetic DNA fragment encoding residues 1–82 from Drosophila melanogaster immune induced molecule 33 (NCBI Reference Sequence: NP_001285594.1) modified at the C terminus to contain an Avitag biotin-ligase site and a 6-His tag (SGLNDIFEAQKIEWHEGHHHHHH) was placed downstream of the cytomegalovirus (CMV) promoter in the mammalian expression vector pFM1.2R by Gibson assembly. Recombinant IM33 protein was produced by transient transfection of Expi293F cells using an ExpiFectamine 293 transfection kit (A14525, Thermo Fisher Scientific). Cell supernatants were harvested 4 days after transfection and concentrated before exchange into 2x PBS at pH 6.5 and finally into 2x PBS at pH 8.0. The soluble recombinant IM33 protein was recovered by 6-His affinity chromatography on Ni-nitrilotriacetic acid (NTA) agarose (786–940, G-Biosciences) and purified by size exclusion chromatography on a Superdex S200 Increase column (28990944, Cytiva).

***E. coli* infection and bacteria load assay—**Prepare the *E. coli* by growing a 2 ml culture of *E. coli* (25922GFP, ATCC) overnight and diluting the bacteria pellet in sterile PBS to approximately 10^9 /ml (Absorbance 600 nm=1). Dip the fine needle into the E.coli solution and prick the flies on one side of the thorax. PBS only was used as the control.

3 hours post-infection each fly was homogenized in 100 μl PBS. 10 μl of homogenate was added to the culture plate and was incubated at 37°C overnight. The CFU was determined by counting the number of colonies.

Bacteria growth assay—10 μl of overnight-grown *E. coli* was added into 2 ml of 2-YT broth (22712020, Thermo Fisher Scientific) and mixed with recombinant IM33 protein to the desired concentration. Grow the bacteria at 37°C for 4 hours and measure the absorbance at 600 nm.

Sleep and locomotion—Except for the thermogenetic experiment, flies were incubated at 24°C under 12h LD cycle. Locomotor activity of flies was monitored by DAM system (Trikinetics) for 5 days at 1 min time interval after the loading day. Flies are considered to be asleep when they do not move for at least 5 minutes. Locomotion counts were calculated using ShinyR-DAM (https://karolcichewicz.shinyapps.io/shinyr-dam/)[50]. Sleep data were processed by custom R-scripts.

Daytime sleep fragmentation—Fly vials (25 flies per vial) were fixed to a rotator (Benchmark Scientific) and were mechanically shaken with the rock model at the maximal speed. The sleep deprivation was conducted from 7 am to 7 pm throughout the lifetime.

Circadian rhythm—After 5-day 12 h LD entrainment, flies were cultured in constant darkness for another 5 days. The locomotion was monitored by DAM system. Circadian rhythmicity was determined by ShinyR-DAM (https://karolcichewicz.shinyapps.io/shinyr-dam/)[50].

Lifespan assay—Flies were collected 3 days after eclosion at a density of 25–30 flies per vial. Every 4 days, the flies were transferred to fresh food, and the number of dead flies was scored. The survival rate was calculated until the death of all flies. At least 4 vials were used for each group.

Climbing assay—Briefly, 10 male flies were transferred to 50 ml cylinders. Flies were tapped down to the bottom of the cylinder, and the climbing behavior was video-recorded. The height of each fly at the 5th second was measured based on the scale of the cylinder. A total of three trials were conducted, and the mean height was calculated.

Immunohistochemistry, imaging and quantifications—Adult brain or gut was dissected in PBS and fixed with 4% PFA for 30 min. After fixation, the samples were washed with 0.3% Triton X-100 in PBS (PBST) for 30 min, followed by incubation in PBST containing 5% BSA for 1 h. The samples were incubated in primary antibodies overnight after the blocking step at 4°C. The primary antibodies used here are: anti-RFP (1:500, PM005, MBL International), anti-Repo (1:100, 8D12, DSHB), anti-HA (1:200, 3724S,

Cell Signaling Technology), anti-Brp (1:100, nc82, DSHB), anti-GFP (1:1000, A-11122, Thermo Fisher Scientific), anti-cleaved Drosophila Dcp-1 (1:100, 9578S, Cell Signaling Technology). After 3-time washes in PBST, fluorescence-conjugated secondary antibodies were used for 2 h at RT, followed by 2-time washes with PBST and a final wash in PBS. The samples were mounted in a mounting medium (H-1200-10, Fisher Scientific). For CaLexA, the fly brains were washed 3 times in PBS after fixation, followed by mounting and imaging.

All the images were acquired using 20x objective under a confocal microscope (Leica, Stellaris) and processed in Fiji. For the quantification of CaLexA signal, identical parameters were used to acquire all the images. ROI management and mean intensity measurement were applied for the quantification.

Dihydroethidium staining—Flies were anesthetized on ice and dissected in Schneider's medium (21-720-024, Fisher Scientific). Brain or gut was incubated in 60 mM Dihydroethidium (37291, Sigma-Aldrich) for 7 minutes in the dark at room temperature, followed by two washes with Schneider's medium and a final wash with PBS. After the washes, the samples were mounted and immediately imaged using a confocal microscope. For quantification, we used the mean of the summed intensities from each tissue, which was then normalized to the area of selection.

TUNEL staining—Adult brains were dissected in PBS and fixed with 4% for 30 min. After fixation, the samples were washed with 0.2% Triton X-100 in PBS for 30 min. The TUNEL staining was performed by following the instructions of DeadEnd fluorometric TUNEL system (G3250, Fisher Scientific).

Calcium imaging—Fly brains were dissected in adult hemolymph-like (AHL) solution (5 mM KCl, 2 mM $CaCl_2$, 8.2 mM $MgCl_2$, 1 mM NaH_2PO_4, 10 mM sucrose, 5 mM trehalose, 5 mM HEPES, 4 mM $NaHCO_3$, pH7.5) and embedded in Agarose L.M.P (16-520-050, Fisher Scientific). After gelation, the samples were immersed in AHL, followed by imaging with a 20X water objective (Olympus). 75 frames were acquired for each sample at the interval of 6.58 seconds and each frame is a maximal projection of 5 z-stack planes. PG or IM33 treatment started from the 26th frame. Each neuron was drawn as an individual ROI, and intensity was quantified in Fiji.

RNA extraction and reverse transcription—15 fly heads or 5 fly bodies or 4 whole flies or 15 fly guts were homogenized in TRIzol reagent (#15596026, Thermo Fisher Scientific) followed by standard phenol-chloroform extraction. After determination of the concentration of RNA, 1 μg of RNA was reverse transcribed to cDNA using the kit (G592, ABM).

Quantitative PCR—The templates and primers were mixed with SYBR green mix solution (BIO-98020, Bioline) and amplified in QuantStudio 6 Flex (Thermo Fisher Scientific). Gene expressions were calculated by the delta-delta Ct method. The primers used here are: IM33 (IM33-F and R), rp49 (rp49-F and R), Dro (Dro-F and R), CecA1 (CecA1-F and R), AtcA (AtcA-F and R), Mtk (Mtk-F and R), Def (Def-F and R), Drs

(Drs-F and R), DptA (DptA-F and R), *L. plantarum* (L. plantarum-F and R),16S rRNA (926F and 1062R).

Drug treatment—Lipoic acid (T5625, Sigma-Aldrich) was dissolved in Ethanol at the final concentration of 2 mM, and 200 μL was applied on the surface of fly food and let dry overnight. THIP (T101-500MG, Sigma-Aldrich) was mixed with standard fly food or DAM food (5% sucrose and 2% Bacto agar (214010, BD)) at the final dosage of 0.1 mg/mL for lifespan assay or sleep assessment respectively. For antibiotic treatment, ampicillin (500 ng/mL, A9518, Sigma-Aldrich), doxycycline (500 ng/mL, D9891, Sigma-Aldrich) and kanamycin (1000 ng/mL, B5264, Sigma-Aldrich) were mixed with autoclaved fly food or DAM food. The microbiota depletion was confirmed by PCR. Purified DAP-type peptidoglycan (69554, Sigma-Aldrich) was dissolved in sterile ddH_2O or AHL at 10 μg/ml concentration for fly feeding or calcium imaging, respectively.

Quantitative analysis of gut bacteria—15 flies are rinsed in 70% ethanol for 3 sec for surface decontamination, followed by gut dissection in sterile PBS. The genomic DNA was extracted by using a DNeasy blood and tissue kit (#69506, Qiagen) in accordance with the manufacturer's instructions. The PCR was performed by using universal primers (27F and 1492R), Acetobacter-specific primers (Aceto-F and R) and Lactobacillus-specific primers (Lacto-F and R). The 16S rRNA sequencing targeting the V4 region was conducted at Genome Analysis and Technology Core in University of Virginia.

Bacteria isolation and transfer—5 flies are rinsed in 70% ethanol for 3 sec and homogenized in 100 μL sterile ddH2O, followed by centrifuge (3000 rpm) for 1 min. 20 μL supernatant was spread on the MRS plate (288210, BD) and incubated at 37°C overnight. Colonies with different morphology were picked and cultured in MRS broth separately (288130, BD). The species was determined by MALDI-TOF MS and further confirmed by sequencing using universal primers 27F and 1492R.

Bacterial cells (approximately 1×10^8) were washed with PBS and added to autoclaved food vials containing ABX-treated or germ-free flies which have been starved for 12 h. All the experiments were performed 3 days post transfer unless otherwise indicated.

CAFE assay—Ten flies were placed into an empty fly vial. Two capillaries of 5 μL (21-180-11, Fisher Scientific) were filled with ddH2O containing 10% sucrose and 1% Indigo carmine (A16052-14, Fisher Scientific) and inserted into the plug of the vial. The flies were left to habituate for one day before measuring the amount of liquid food for the following three consecutive days. The capillaries were replaced every 24 hours.

Glucose measurement—We followed the protocol described previouly[51]. Briefly, 5 adult flies were homogenized in 100 μl of cold PBS. 10 μl of the homogenate was used to measure the protein content by BCA protein assay kit (23225, Fisher Scientific). After heating (70°C for 10 min) and centrifuge (14000 rpm), 30 μl of supernatant were added to 100 μl of HK (GAHK20-1KT, Sigma-Aldrich) solution followed by the absorbance reading at 340 nm.

Triglyceride measurement—According to the published protocol[51], 5 adult flies were homogenized in 100 μl of PBS with 0.05% Tween 20. Pipette 10 μl of homogenized sample to measure protein content with BCA protein assay kit (23225, Fisher Scientific). Mix 20 μl of sample with 20 μl of triglyceride reagent (T2449, Sigma-Aldrich) and incubate 37 °C for 60 min. Add 30 μl of mixed solution to 100 μl of free glycerol reagent (F6428, Sigma-Aldrich) and read the absorbance at 540 nm.

Singe-cell RNA sequencing preparation—18 fly brains per group were dissected in cold Schneider's medium (21-720-024, Fisher Scientific) and transferred to 1.5 ml tube with Schneider's medium on ice. Briefly centrifuge the brain to the bottom of the tube and wash with DPBS for 3 times. Add 300 ul digesting solution containing papain (100 unit/mL, LK003178, Worthington Biochemical) and collagenase I (1.11 mg/mL, C2674, Sigma-Aldrich) to brain samples, incubate in tube shaker 25 °C with 1000 rpm for 20 min (pipet the solution up and down 30 times every 5 min). Stop the digestion by adding 400 ul cold Schneider's medium to the tube and elute the solution to 5 ml tubes through 40 um cell strainer. Centrifuge (600 rpm) for 6 min and discard the supernatant. Resuspend the pellet with fluorescence-activated cell sorting (FACS) buffer (PBS with 2% BSA) containing SYTOX green (R37168, Thermo Fisher Scientific). GFP- cells were FACS sorted (BD Biosciences) and utilized for scRNA sequencing. Sample loading and library construction were performed using the 10X Genomics Chromium platform as previously described[17].

16S rRNA sequence analysis—16S rRNA reads were processed using the DADA2 pipeline (v1.17.3) in R v4.0.3[52], which incorporates quality-filtering, dereplication, and removal of chimeric sequences, to identify amplicon sequence variants (ASVs). The R package DECIPHER (v2.16.1)[53] was used in conjunction with the SILVA SSU rRNA database (release 138)[54] for taxonomic assignation of the ASVs. Contaminant eukaryotic reads from spuriously amplified *Drosophila* DNA were removed. Rarefaction analysis was performed using the vegan package (v2.2–7) in R[55]. Briefly, for each sample ASV counts were subsampled to depths of 1, 100, 1000, 5000, and 10000:160000 in 10000 count increments, and alpha diversity ('richness', or number of unique observed ASVs) was calculated at each depth. Pairwise Wilcoxon tests between all subsampling depths for differences in alpha diversity were then carried out, with Bejamini-Hochberg adjustment for multiple hypothesis testing. The read threshold was defined as the lowest read depth at which there was no significant difference in sample alpha diversities compared to any higher read depth. All samples passed the empirically determined read threshold (50,000 reads) and were thus retained in downstream analyses. The R package phyloseq (v1.32.0)[56] was used to collate the DADA2 output (ASV counts and taxonomic identity) with sample metadata in order to calculate relative abundances of ASVs per sample (counts of each unique ASV divided by total ASV counts for a sample), and compare ASV relative abundances between treatment groups. The data set was filtered to exclude lowly incident ASVs observed in only a single sample. To identify ASVs significantly associated with experimental group, linear models were fit to log transformed ASV relative abundances as implemented in the MaAsLin2 (v1.2.0) R package[57], with 'Group' as the only fixed effect and no random effects. Other specified parameters included min_prevalence = 0.1 (filtering for ASVs observed in at least 10% of samples) and max_significance = 0.05

(restricting significant results to those with Benjamini-Hochberg adjusted p-values < 0.05). The DECIPHER pipeline for taxonomic assignation using the SILVA SSU rRNA database rarely results in taxonomic identification of ASVs at the species level. Therefore ASV sequences significantly associated with experimental groups were submitted to NCBI blastn against the nr/nt database for highly similar sequences using default search parameters. Species-level taxonomies were assigned to significant ASVs if the high-identity search hits (>99%) were unambiguous with all hits pertaining to the same species.

Single-cell data analysis

Preprocessing: Reads were aligned to the dm6 genome using the Cellranger software pipeline (version 6.0.0) provided by 10x genomics. The resulting filtered gene by cell matrices of UMI counts for each sample were read into R using the read10xCounts function from the Droplet Utils package. Filtering was applied in order to remove low quality cells by excluding cells expressing fewer than 200 or greater than 4,000 unique genes, having fewer than 1,000 or greater than 50,000 UMI counts, as well as cells with greater than 25% mitochondrial gene expression. Expression values for the remaining cells were then merged by gene symbol into one dataframe and normalized using the scran and scater packages. The resulting log2 values were transformed to the natural log scale for compatibility with the Seurat (v3) pipeline[58–60].

Dimensionality reduction and clustering: The filtered and normalized matrix was used as input to the Seurat pipeline and cells were scaled across each gene before the selection of the top 2,000 most highly variable genes using variance stabilizing transformation. Principal Components Analysis was conducted and an elbow plot was used to select the first thirty principal components for tSNE analysis and clustering. Shared Nearest Neighbor (SNN) clustering optimized with the Louvain algorithm, as implemented by the Seurat FindClusters function was performed before manual annotation of clusters based on expression of canonical gene markers.

Differential expression: For analysis of differentially expressed genes between conditions, each cluster was filtered to include genes that had at least 5 transcripts in at least 5 cells, then the top 2000 highly variable genes were determined and included for further analysis using the SingleCellExperiment modelGeneVar and getTopHVGs functions. After filtering, observational weights for each gene were calculated using the ZINB-WaVE zinbFit and zinbwave functions[61]. These were then included in the edgeR model, which was created with the glmFit function, by using the glmWeightedF function[62]. Results were then filtered using a Benjamini-Hochberg adjusted p-value threshold of less than 0.05 as statistically significant.

Pathway enrichment: Over representation enrichment analysis with Fisher's Exact test was used to determine significantly enriched Gene Ontology (GO) terms (adj. p < 0.05) for the sets of significantly differentially expressed genes. For each gene set, genes were separated into up- and downregulated and separately[63] the enrichGO function from the clusterProfiler package was used with a gene set size set between 10 and 500 genes and p-values adjusted using the Benjamini-Hochberg correction[64].

Quantification and statistical analysis

Data analysis and statistics were carried out using GraphPad Prism 9 (GraphPad Software Inc.). Data are presented as Mean ± S.E.M.. Comparisons of the two groups were made by unpaired two-tailed t-test. Comparisons of multiple groups were made by one-way ANOVA with Tukey's multi-comparisons test. Comparisons of multiple factors, two-way ANOVA with Sidak's multiple-comparisons tests were used. P values < 0.05 were considered statistically significant.

Supplementary Material

Refer to Web version on PubMed Central for supplementary material.

Acknowledgments

We would like to thank Shirley Smith for editing the manuscript. We thank Dr. Sarah Ackerman for the critical reading and suggestions. We thank Dr. Paul Shaw for the valuable suggestions. Stocks obtained from the Bloomington Drosophila Stock Center (NIH P40OD018537) were used in this study. We thank all the members of the Kipnis lab for their valuable feedback during multiple discussions of this work. We thank Washington University in St. Louis Department of Pathology and Immunology Flow Cytometry and Fluorescence Activated Cell Sorting Core for help with cell sorting. We thank the University of Virginia Genome Analysis and Technology Core for help with 16S rRNA sequencing. We thank the Washington University in St. Louis McDonnell Genome Institute (MGI) for help with single-cell RNA-seq library preparation and sequencing. This work was supported by grants from the National Center for Complementary and Integrative Health DP1AT010416 to J.K., NIAID HHSN272201700060C to D.F. and R01-AT009741 to G.D.

Inclusion and diversity

We support inclusive, diverse, and equitable conduct of research.

References

1. Lopez-Otin C, Blasco MA, Partridge L, Serrano M, and Kroemer G (2013). The hallmarks of aging. Cell 153, 1194–1217. 10.1016/j.cell.2013.05.039. [PubMed: 23746838]
2. Nikolich-Zugich J (2018). The twilight of immunity: emerging concepts in aging of the immune system. Nat Immunol 19, 10–19. 10.1038/s41590-017-0006-x. [PubMed: 29242543]
3. Lazzaro BP, Zasloff M, and Rolff J (2020). Antimicrobial peptides: Application informed by evolution. Science 368, eaau5480. 10.1126/science.aau5480. [PubMed: 32355003]
4. Zhang L. j., and Gallo RL (2016). Antimicrobial peptides. Current Biology 26, R14–R19. 10.1016/j.cub.2015.11.017. [PubMed: 26766224]
5. Hanson MA, and Lemaitre B (2020). New insights on Drosophila antimicrobial peptide function in host defense and beyond. Curr Opin Immunol 62, 22–30. 10.1016/j.coi.2019.11.008. [PubMed: 31835066]
6. Su Y, Zhang K, and Schluesener HJ (2010). Antimicrobial peptides in the brain. Arch Immunol Ther Exp (Warsz) 58, 365–377. 10.1007/s00005-010-0089-7. [PubMed: 20668978]
7. Lopez-Otin C, Blasco MA, Partridge L, Serrano M, and Kroemer G (2023). Hallmarks of aging: An expanding universe. Cell 186, 243–278. 10.1016/j.cell.2022.11.001. [PubMed: 36599349]
8. Ghosh TS, Shanahan F, and O'Toole PW (2022). The gut microbiome as a modulator of healthy ageing. Nat Rev Gastro Hepat 19, 565–584. 10.1038/s41575-022-00605-x.
9. Tracey KJ (2002). The inflammatory reflex. Nature 420, 853–859. 10.1038/nature01321. [PubMed: 12490958]
10. Vaccaro A, Dor YK, Nambara K, Pollina EA, Lin CD, Greenberg ME, and Rogulja D (2020). Sleep Loss Can Cause Death through Accumulation of Reactive Oxygen Species in the Gut. Cell 181, 1307–+. 10.1016/j.cell.2020.04.049. [PubMed: 32502393]

11. Mayer EA, Nance K, and Chen S (2022). The Gut–Brain Axis. Annual Review of Medicine 73, 439–453. 10.1146/annurev-med-042320-014032.
12. Nagpal J, and Cryan JF (2021). Microbiota-brain interactions: Moving toward mechanisms in model organisms. Neuron. 10.1016/j.neuron.2021.09.036.
13. Vuong HE, Yano JM, Fung TC, and Hsiao EY (2017). The Microbiome and Host Behavior. Annu Rev Neurosci 40, 21–49. 10.1146/annurev-neuro-072116-031347. [PubMed: 28301775]
14. Mattis J, and Sehgal A (2016). Circadian Rhythms, Sleep, and Disorders of Aging. Trends Endocrinol Metab 27, 192–203. 10.1016/j.tem.2016.02.003. [PubMed: 26947521]
15. Mander BA, Winer JR, and Walker MP (2017). Sleep and Human Aging. Neuron 94, 19–36. 10.1016/j.neuron.2017.02.004. [PubMed: 28384471]
16. Koh K, Evans JM, Hendricks JC, and Sehgal A (2006). A Drosophila model for age-associated changes in sleep:wake cycles. Proc Natl Acad Sci U S A 103, 13843–13847. 10.1073/pnas.0605903103. [PubMed: 16938867]
17. Rustenhoven J, Drieu A, Mamuladze T, de Lima KA, Dykstra T, Wall M, Papadopoulos Z, Kanamori M, Salvador AF, Baker W, et al. (2021). Functional characterization of the dural sinuses as a neuroimmune interface. Cell 184, 1000–+. 10.1016/j.cell.2020.12.040. [PubMed: 33508229]
18. Nicholson L, Singh GK, Osterwalder T, Roman GW, Davis RL, and Keshishian H (2008). Spatial and temporal control of gene expression in drosophila using the inducible GeneSwitch GAL4 system. I. Screen for larval nervous system drivers. Genetics 178, 215–234. 10.1534/genetics.107.081968. [PubMed: 18202369]
19. Lee KM, Mathies LD, and Grotewiel M (2019). Alcohol sedation in adult Drosophila is regulated by Cysteine proteinase-1 in cortex glia. Commun Biol 2, 252. 10.1038/s42003-019-0492-5. [PubMed: 31286069]
20. Levy F, Rabel D, Charlet M, Bulet P, Hoffmann JA, and Ehret-Sabatier L (2004). Peptidomic and proteomic analyses of the systemic immune response of Drosophila. Biochimie 86, 607–616. 10.1016/j.biochi.2004.07.007. [PubMed: 15556270]
21. Obata F, Fons CO, and Gould AP (2018). Early-life exposure to low-dose oxidants can increase longevity via microbiome remodelling in Drosophila. Nat Commun 9, 975. 10.1038/s41467-018-03070-w. [PubMed: 29515102]
22. Gould AL, Zhang V, Lamberti L, Jones EW, Obadia B, Korasidis N, Gavryushkin A, Carlson JM, Beerenwinkel N, and Ludington WB (2018). Microbiome interactions shape host fitness. Proc Natl Acad Sci U S A 115, E11951–E11960. 10.1073/pnas.1809349115. [PubMed: 30510004]
23. Fast D, Duggal A, and Foley E (2018). Monoassociation with Lactobacillus plantarum Disrupts Intestinal Homeostasis in Adult Drosophila melanogaster. mBio 9. 10.1128/mBio.01114-18.
24. Iatsenko I, Boquete JP, and Lemaitre B (2018). Microbiota-Derived Lactate Activates Production of Reactive Oxygen Species by the Intestinal NADPH Oxidase Nox and Shortens Drosophila Lifespan. Immunity 49, 929–942 e925. 10.1016/j.immuni.2018.09.017. [PubMed: 30446385]
25. Sharon G, Sampson TR, Geschwind DH, and Mazmanian SK (2016). The Central Nervous System and the Gut Microbiome. Cell 167, 915–932. 10.1016/j.cell.2016.10.027. [PubMed: 27814521]
26. Dissel S, Angadi V, Kirszenblat L, Suzuki Y, Donlea J, Klose M, Koch Z, English D, Winsky-Sommerer R, van Swinderen B, and Shaw PJ (2015). Sleep restores behavioral plasticity to Drosophila mutants. Current biology : CB 25, 1270–1281. 10.1016/j.cub.2015.03.027. [PubMed: 25913403]
27. Donlea JM, Thimgan MS, Suzuki Y, Gottschalk L, and Shaw PJ (2011). Inducing sleep by remote control facilitates memory consolidation in Drosophila. Science 332, 1571–1576. 10.1126/science.1202249. [PubMed: 21700877]
28. Hill VM, O'Connor RM, Sissoko GB, Irobunda IS, Leong S, Canman JC, Stavropoulos N, and Shirasu-Hiza M (2018). A bidirectional relationship between sleep and oxidative stress in Drosophila. Plos Biology 16. ARTN e2005206 10.1371/journal.pbio.2005206.
29. Schretter CE, Vielmetter J, Bartos I, Marka Z, Marka S, Argade S, and Mazmanian SK (2018). A gut microbial factor modulates locomotor behaviour in Drosophila. Nature 563, 402–406. 10.1038/s41586-018-0634-9. [PubMed: 30356215]
30. Davie K, Janssens J, Koldere D, De Waegeneer M, Pech U, Kreft L, Aibar S, Makhzami S, Christiaens V, Bravo Gonzalez-Blas C, et al. (2018). A Single-Cell Transcriptome Atlas

of the Aging Drosophila Brain. Cell 174, 982–998 e920. 10.1016/j.cell.2018.05.057. [PubMed: 29909982]

31. Dubowy C, and Sehgal A (2017). Circadian Rhythms and Sleep in Drosophila melanogaster. Genetics 205, 1373–1397. 10.1534/genetics.115.185157. [PubMed: 28360128]
32. Crocker A, Shahidullah M, Levitan IB, and Sehgal A (2010). Identification of a Neural Circuit that Underlies the Effects of Octopamine on Sleep:Wake Behavior. Neuron 65, 670–681. 10.1016/j.neuron.2010.01.032. [PubMed: 20223202]
33. Masuyama K, Zhang Y, Rao Y, and Wang JW (2012). Mapping neural circuits with activity-dependent nuclear import of a transcription factor. J Neurogenet 26, 89–102. 10.3109/01677063.2011.642910. [PubMed: 22236090]
34. Kitamoto T (2001). Conditional modification of behavior in Drosophila by targeted expression of a temperature-sensitive shibire allele in defined neurons. J Neurobiol 47, 81–92. 10.1002/neu.1018. [PubMed: 11291099]
35. Lesperance DNA, and Broderick NA (2020). Microbiomes as modulators of Drosophila melanogaster homeostasis and disease. Curr Opin Insect Sci 39, 84–90. 10.1016/j.cois.2020.03.003. [PubMed: 32339931]
36. Kurz CL, Charroux B, Chaduli D, Viallat-Lieutaud A, and Royet J (2017). Peptidoglycan sensing by octopaminergic neurons modulates Drosophila oviposition. Elife 6. 10.7554/eLife.21937.
37. Gabanyi I, Lepousez G, Wheeler R, Vieites-Prado A, Nissant A, Wagner S, Moigneu C, Dulauroy S, Hicham S, Polomack B, et al. (2022). Bacterial sensing via neuronal Nod2 regulates appetite and body temperature. Science 376, eabj3986. 10.1126/science.abj3986. [PubMed: 35420957]
38. Kounatidis I, Chtarbanova S, Cao Y, Hayne M, Jayanth D, Ganetzky B, and Ligoxygakis P (2017). NF-kappaB Immunity in the Brain Determines Fly Lifespan in Healthy Aging and Age-Related Neurodegeneration. Cell Rep 19, 836–848. 10.1016/j.celrep.2017.04.007. [PubMed: 28445733]
39. Cao Y, Chtarbanova S, Petersen AJ, and Ganetzky B (2013). Dnr1 mutations cause neurodegeneration in Drosophila by activating the innate immune response in the brain. Proc Natl Acad Sci U S A 110, E1752–1760. 10.1073/pnas.1306220110. [PubMed: 23613578]
40. Sinner MP, Masurat F, Ewbank JJ, Pujol N, and Bringmann H (2020). Innate Immunity Promotes Sleep through Epidermal Antimicrobial Peptides. Current biology : CB. 10.1016/j.cub.2020.10.076.
41. Ha EM, Oh CT, Bae YS, and Lee WJ (2005). A direct role for dual oxidase in Drosophila gut immunity. Science 310, 847–850. 10.1126/science.1117311. [PubMed: 16272120]
42. Zhang Y, Li Y, Barber AF, Noya SB, Williams JA, Li F, Daniel SG, Bittinger K, Fang J, and Sehgal A (2023). The microbiome stabilizes circadian rhythms in the gut. Proc Natl Acad Sci U S A 120, e2217532120. 10.1073/pnas.2217532120. [PubMed: 36689661]
43. Bishehsari F, Voigt RM, and Keshavarzian A (2020). Circadian rhythms and the gut microbiota: from the metabolic syndrome to cancer. Nat Rev Endocrinol 16, 731–739. 10.1038/s41574-020-00427-4. [PubMed: 33106657]
44. Kim B, Kanai MI, Oh Y, Kyung M, Kim EK, Jang IH, Lee JH, Kim SG, Suh GSB, and Lee WJ (2021). Response of the microbiome-gut-brain axis in Drosophila to amino acid deficit. Nature. 10.1038/s41586-021-03522-2.
45. Davis DJ, Doerr HM, Grzelak AK, Busi SB, Jasarevic E, Ericsson AC, and Bryda EC (2016). Lactobacillus plantarum attenuates anxiety-related behavior and protects against stress-induced dysbiosis in adult zebrafish. Sci Rep 6, 33726. 10.1038/srep33726. [PubMed: 27641717]
46. Liu G, Chong HX, Chung FY, Li Y, and Liong MT (2020). Lactobacillus plantarum DR7 Modulated Bowel Movement and Gut Microbiota Associated with Dopamine and Serotonin Pathways in Stressed Adults. Int J Mol Sci 21. 10.3390/ijms21134608.
47. Gonzalez-Santana A, and Diaz Heijtz R (2020). Bacterial Peptidoglycans from Microbiota in Neurodevelopment and Behavior. Trends Mol Med 26, 729–743. 10.1016/j.molmed.2020.05.003. [PubMed: 32507655]
48. Gratz SJ, Rubinstein CD, Harrison MM, Wildonger J, and O'Connor-Giles KM (2015). CRISPR-Cas9 Genome Editing in Drosophila. Curr Protoc Mol Biol 111, 31 32 31–20. 10.1002/0471142727.mb3102s111.

49. Koyle ML, Veloz M, Judd AM, Wong AC, Newell PD, Douglas AE, and Chaston JM (2016). Rearing the Fruit Fly Drosophila melanogaster Under Axenic and Gnotobiotic Conditions. Journal of visualized experiments : JoVE. 10.3791/54219.
50. Cichewicz K, and Hirsh J (2018). ShinyR-DAM: a program analyzing Drosophila activity, sleep and circadian rhythms. Communications Biology 1, 25. 10.1038/s42003-018-0031-9. [PubMed: 29911688]
51. Tennessen JM, Barry WE, Cox J, and Thummel CS (2014). Methods for studying metabolism in Drosophila. Methods 68, 105–115. 10.1016/j.ymeth.2014.02.034. [PubMed: 24631891]
52. Callahan BJ, McMurdie PJ, Rosen MJ, Han AW, Johnson AJA, and Holmes SP (2016). DADA2: High-resolution sample inference from Illumina amplicon data. Nature Methods 13, 581–583. 10.1038/nmeth.3869. [PubMed: 27214047]
53. Wright ES (2015). DECIPHER: harnessing local sequence context to improve protein multiple sequence alignment. BMC Bioinformatics 16, 322. 10.1186/s12859-015-0749-z. [PubMed: 26445311]
54. Quast C, Pruesse E, Yilmaz P, Gerken J, Schweer T, Yarza P, Peplies J, and Glockner FO (2013). The SILVA ribosomal RNA gene database project: improved data processing and web-based tools. Nucleic Acids Res 41, D590–596. 10.1093/nar/gks1219. [PubMed: 23193283]
55. Oksanen J, Blanchet FG, Friendly M, Kindt R, Legendre P, McGlinn D, Minchin PR, O'Hara RB, Simpson GL, Solymos P, et al. (2016). vegan: Community Ecology Package. Ordination methods, diversity analysis and other functions for community and vegetation ecologists.
56. McMurdie PJ, and Holmes S (2013). phyloseq: an R package for reproducible interactive analysis and graphics of microbiome census data. PLoS One 8, e61217. 10.1371/journal.pone.0061217. [PubMed: 23630581]
57. Mallick H, Rahnavard A, McIver LJ, Ma S, Zhang Y, Nguyen LH, Tickle TL, Weingart G, Ren B, Schwager EH, et al. (2021). Multivariable Association Discovery in Population-scale Meta-omics Studies. bioRxiv, 2021.2001.2020.427420. 10.1101/2021.01.20.427420.
58. McCarthy DJ, Campbell KR, Lun AT, and Wills QF (2017). Scater: pre-processing, quality control, normalization and visualization of single-cell RNA-seq data in R. Bioinformatics 33, 1179–1186. 10.1093/bioinformatics/btw777. [PubMed: 28088763]
59. Lun AT, McCarthy DJ, and Marioni JC (2016). A step-by-step workflow for low-level analysis of single-cell RNA-seq data with Bioconductor. F1000Res 5, 2122. 10.12688/f1000research.9501.2. [PubMed: 27909575]
60. Butler A, Hoffman P, Smibert P, Papalexi E, and Satija R (2018). Integrating single-cell transcriptomic data across different conditions, technologies, and species. Nat Biotechnol 36, 411–420. 10.1038/nbt.4096. [PubMed: 29608179]
61. Van den Berge K, Perraudeau F, Soneson C, Love MI, Risso D, Vert JP, Robinson MD, Dudoit S, and Clement L (2018). Observation weights unlock bulk RNA-seq tools for zero inflation and single-cell applications. Genome biology 19, 24. 10.1186/s13059-018-1406-4. [PubMed: 29478411]
62. Robinson MD, McCarthy DJ, and Smyth GK (2010). edgeR: a Bioconductor package for differential expression analysis of digital gene expression data. Bioinformatics 26, 139–140. 10.1093/bioinformatics/btp616. [PubMed: 19910308]
63. Hong G, Zhang W, Li H, Shen X, and Guo Z (2014). Separate enrichment analysis of pathways for up- and downregulated genes. J R Soc Interface 11, 20130950. 10.1098/rsif.2013.0950. [PubMed: 24352673]
64. Yu GC, Wang LG, Han YY, and He QY (2012). clusterProfiler: an R Package for Comparing Biological Themes Among Gene Clusters. Omics 16, 284–287. 10.1089/omi.2011.0118. [PubMed: 22455463]

Highlights

- Glia-derived IM33 is sufficient and necessary to control lifespan
- Glia-derived IM33 sustains lifespan by the control of gut microbiota and ROS
- Glia-derived IM33 modulates sleep through gut *L. plantarum*
- *L. plantarum*-derived peptidoglycan activates insulin-producing cells to modulate sleep

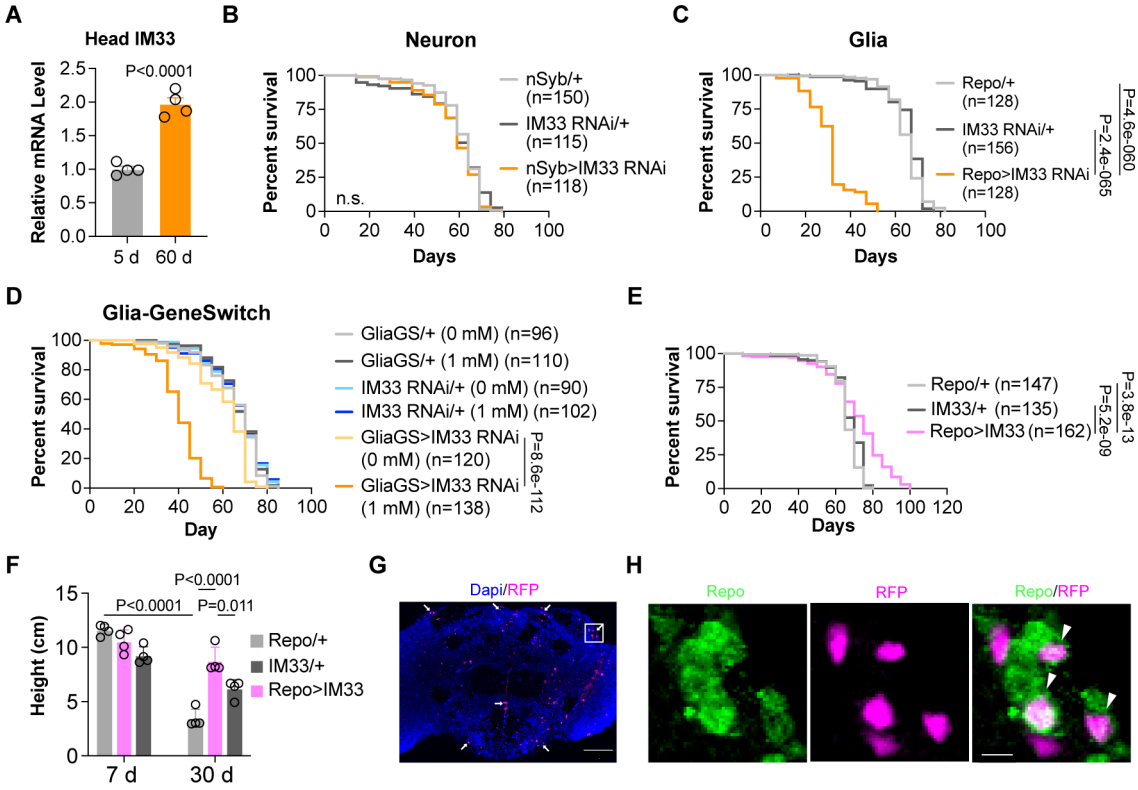

Figure 1. Glia-derived IM33 is required to maintain the lifespan.

(A) Relative mRNA level of head IM33 of young and old wild-type flies. Mean ± S.E.M.. Two-tailed unpaired t-test. Each dot represents a pool of 15 fly heads. (B and C) The lifespan of flies with neuronal (B) or glial (C) knockdown of IM33. Log-rank test. (D) Knockdown of IM33 in glia from the adulthood stage shortens the lifespan. Log-rank test. (E) The lifespan of control (Repo/+, IM33/+) and IM33-overexpressing flies (Repo>IM33). Log-rank test. (F) Climbing assay of young (7 d) and old (30 d) flies with indicated genotype. Mean ± S.E.M.. Two-way ANOVA with Sidak's multiple-comparisons test. Each dot represents one testing vial that contains 10 flies. (G) Representative images showing the staining of RFP and Dapi of the fly brain. Arrows indicate the areas enriched with RFP-positive cells at the brain border. Genotype: IM33-Gal4>UAS-RedStinger. Scale bar: 50 μm. (H) Double staining of RFP and glia marker Repo of the brain area highlighted in (G). Arrowheads indicate the RFP+ cells colocalized with Repo. Scale bar: 5 μm.

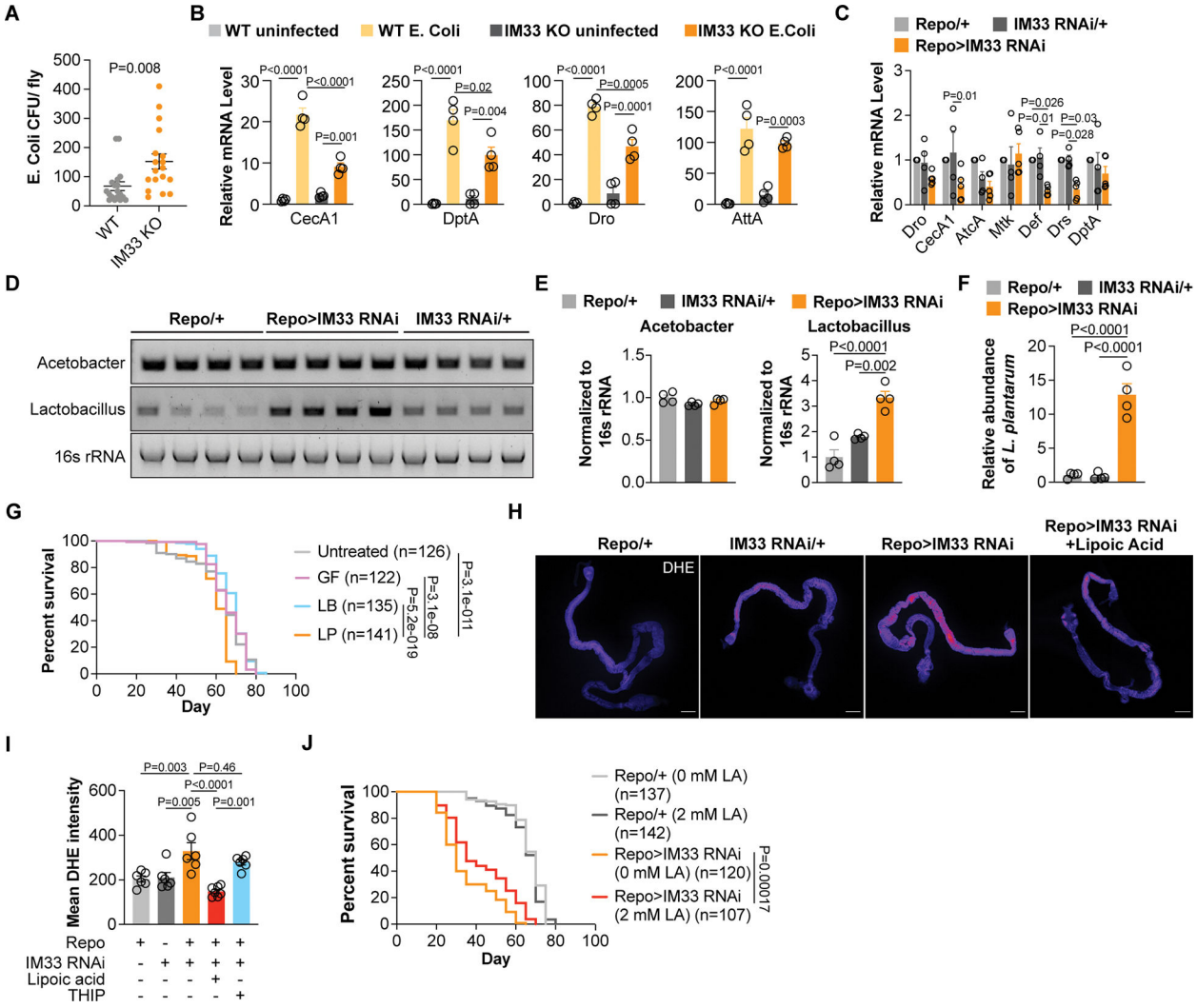

Figure 2. Glia-derived IM33 shapes the gut microbiota via immune modulation.

(A) The number of colony-forming units (CFU) in wild-type and IM33 deficient flies 3 h post-E. coli infection. Mean ± S.E.M.. Two-tailed unpaired t-test. Each dot represents one fly. (B) The relative mRNA abundance of anti-Gram negative antimicrobial peptides in wild-type and IM33 knockout flies with or without E. coli infection. Mean ± S.E.M.. One-way ANOVA with Tukey's multiple-comparisons test. Each dot represents a pool of 4 flies. (C) The relative mRNA level of gut AMPs of control (Repo/+, IM33 RNAi/+) or glial IM33-deficient flies (Repo>IM33 RNAi). Mean ± S.E.M.. Two-way ANOVA with Sidak's multiple-comparisons test. Each dot represents a pool of 15 fly guts. (D) PCR of Acetobacter and Lactobacillus from control or IM33 RNAi fly gut. (E) The quantification of (D). Mean ± S.E.M.. One-way ANOVA with Tukey's multiple-comparisons test. Each dot represents a pool of 15 fly guts. (F) qPCR of *L. plantarum* abundance in flies with glial IM33 knockdown. One-way ANOVA with Tukey's multiple-comparisons test. Each dot represents a pool of 15 fly guts. (G) The lifespan of flies with intact microbiota (untreated), microbiota depletion (ABX), *L. brevis* (LB) or *L. plantarum* (LP). Log-rank test. (H) Representative images of DHE staining of the gut from flies with indicated genotype

and treatment. Scale bar: 200 μm. (I) Quantification of the gut DHE fluorescence of flies with indicated genotype and treatment. Mean ± S.E.M.. One-way ANOVA with Tukey's multiple-comparisons test. Each dot represents one fly gut. (J) Lipoic acid (LA) treatment extends the lifespan of the flies with glial IM33 knockdown. Log-rank test.

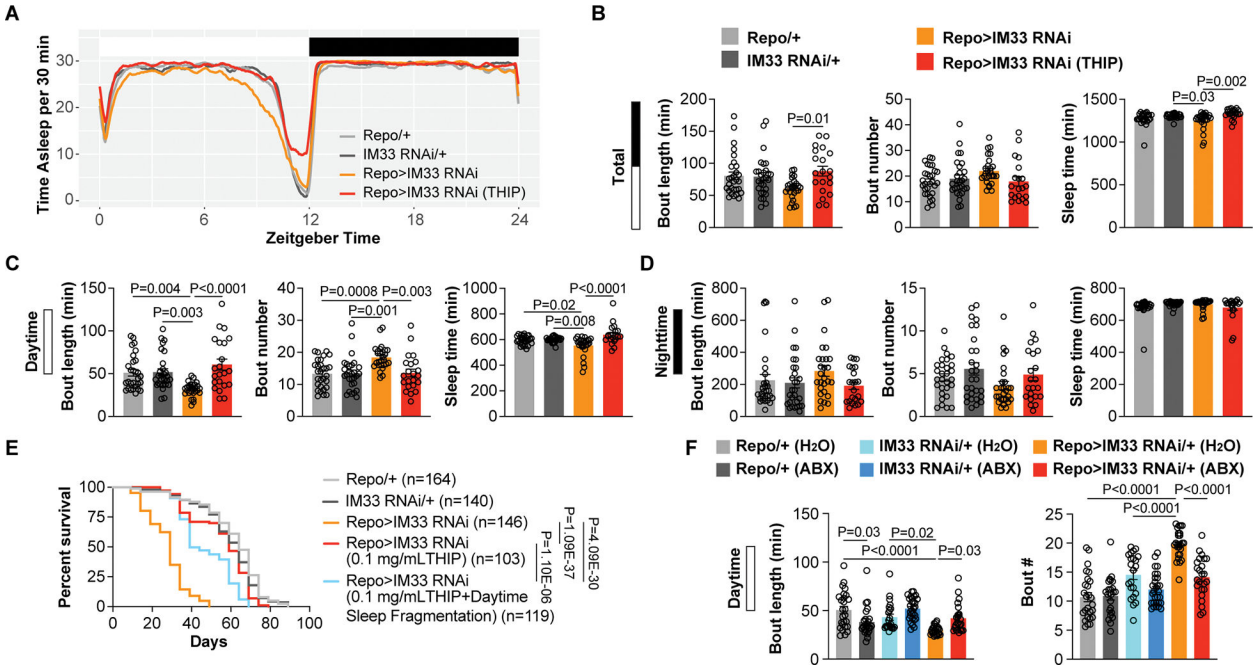

Figure 3. Glia-derived IM33 modulates sleep in a microbiota-dependent manner.

(A) Sleep profiles of flies with indicated genotype and treatment. (B-D) Quantification of total (B), daytime (C) and nighttime (D) sleep bout length, sleep bout number and sleep time in (A). Mean ± S.E.M.. One-way ANOVA with Tukey's multiple-comparisons test. Each dot represents one fly. (E) Survival curves of flies with indicated genotype and treatment. Log-rank test. (F) Quantification of daytime sleep bout length and number of flies with indicated genotype and treatment. Mean ± S.E.M.. One-way ANOVA with Tukey's multiple-comparisons test. Each dot represents one fly.

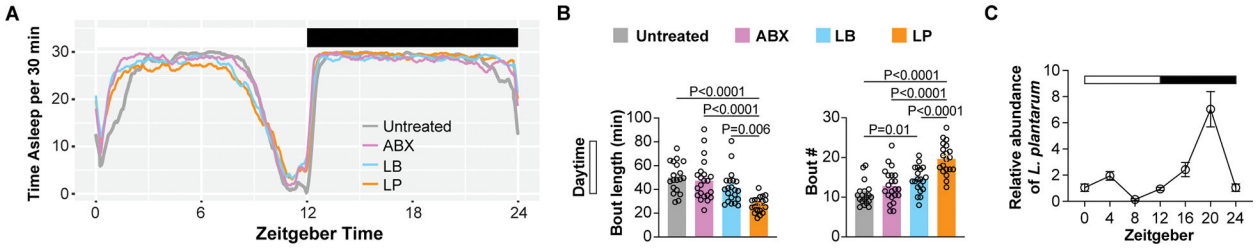

Figure 4. The daytime sleep regulation by glial IM33 is mediated by *L. plantarum*.

(A) Sleep profiles of untreated flies, flies with ABX treatment, and flies transferred with *L. brevis* (LB) or *L. plantarum* (LP). (B) Quantification of daytime sleep quality in (A). Mean ± S.E.M.. One-way ANOVA with Tukey's multiple-comparisons test. Each dot represents one fly. (C) The abundance of *L. plantarum* from ZT0-ZT24 at 4-hour intervals. Mean ± S.E.M.. N=4 for each time point, each N is a pool of 15 fly guts.

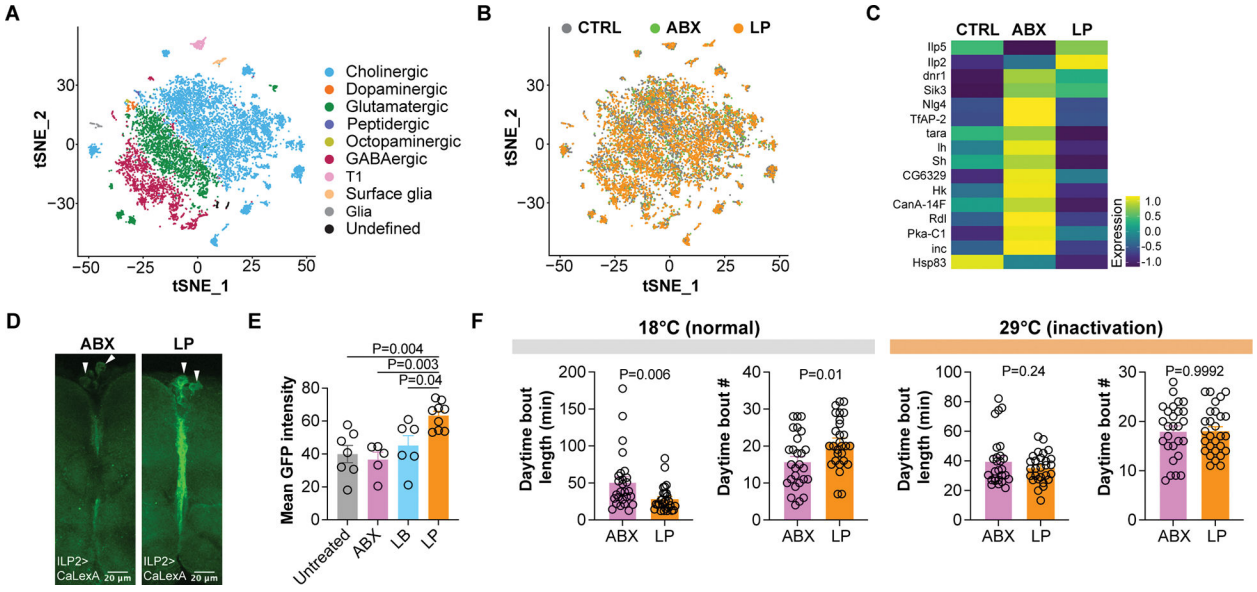

Figure 5. The activation of insulin-producing cells by *L. plantarum* causes daytime sleep fragmentation.

(A) tSNE plot of all the samples with annotated clusters. (B) tSNE plot of the three samples with indicated color. (C) Heatmap showing the average scaled expression of sleep-related genes in the three groups. (D) The natural CaLexA signal in IPCs after ABX treatment or *L. plantarum* transfer. Arrowheads indicate the IPCs. Scale bar: 20 μm. (E) Quantification of the CaLexA intensity in the cell bodies of IPCs from flies with indicated treatment. Mean ± S.E.M.. One-way ANOVA with Tukey's multiple-comparisons test. Each dot represents one fly brain. (F) Quantification of the daytime sleep bout length and number under indicated conditions. Genotype: ILP2>Shibire^{ts}. Mean ± S.E.M.. Two-tailed unpaired t-test. Each dot represents one fly. LP: *L. plantarum*; LB: *L. brevis.*

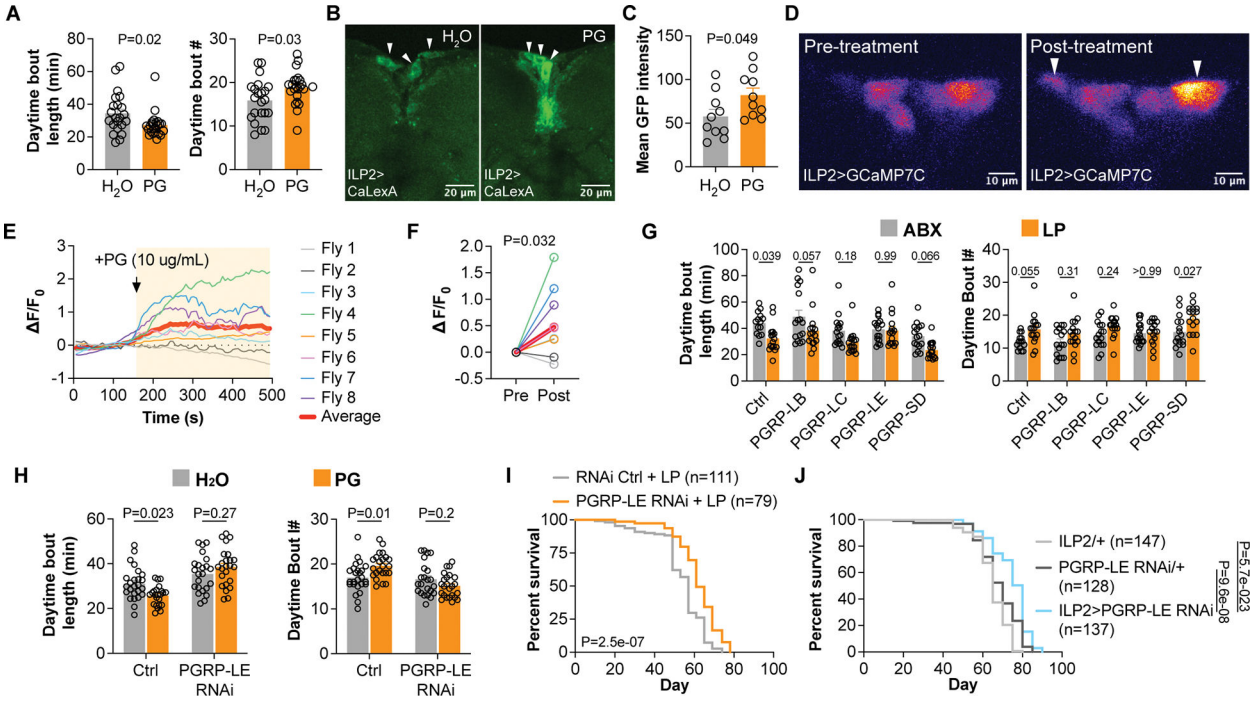

Figure 6. *L. plantarum*-derived peptidoglycan signals on PGRP-LE to activate IPCs.

(A) Quantification of the daytime sleep bout length and number of flies fed with water or DAP-type peptidoglycan (10 ug/ml). Mean ± S.E.M.. Two-tailed unpaired t-test. Each dot represents one fly. (B) Representative images showing the CaLexA signal in IPCs from water-treated or PG-treated flies. Scale bar: 20 μm. (C) Quantification of the CaLexA intensity in the cell bodies of IPCs from flies with or without PG. Mean ± S.E.M.. Two-tailed unpaired t-test. Each dot represents one fly brain. (D) Representative images of GCaMP7c signal in IPCs in the absence or presence of peptidoglycan. Scale bar: 10 μm. (E) Traces of GCaMP7c signal in IPCs upon peptidoglycan treatment. (F) Quantification of the normalized GCaMP7c signal in IPCs before and after PG treatment. Paired t-test. Each dot pair represents one fly brain. (G) *L. plantarum* transfer-induced daytime sleep fragmentation is prevented by PGRP-LE knockdown in IPCs. Mean ± S.E.M.. Two-way ANOVA with Sidak's multiple-comparisons test. Each dot represents one fly. (H) Knockdown of PGRP-LE in IPCs blocks the PG treatment-induced daytime sleep fragmentation. Mean ± S.E.M.. Two-way ANOVA with Sidak's multiple-comparisons test. Each dot represents one fly. (I) Knockdown of PGRP-LE in IPCs rescues the *L. plantarum* transfer-caused shortened lifespan. Log-rank test. (J) Survival curve of flies with indicated genotype. Log-rank test. LP: *L. plantarum.*

Key resources table

REAGENT or RESOURCE	SOURCE	IDENTIFIER
Antibodies		
Rabbit polyclonal anti-RFP	MBL International	Cat# PM005, RRID:AB_591279
Mouse monoclonal anti-Repo	DSHB	Cat# 8D12 RRID:AB_528448
Rabbit monoclonal anti-HA	Cell Signaling Technology	Cat# 3724, RRID:AB_1549585
Mouse monoclonal anti-Brp	DSHB	Cat# nc82, RRID:AB_2314866
Rabbit polyclonal anti-cleaved Dcp-1	Cell Signaling Technology	Cat# 9578, RRID:AB_2721060
Rabbit polyclonal anti-GFP	Thermo Fisher Scientific	Cat# A-11122, RRID:AB_221569
Bacterial and virus strains		
GFP-Escherichia coli	ATCC	ATCC 25922GFP
L. plantarum	This paper	
L. brevis	This paper	
Chemicals, peptides, and recombinant proteins		
RU486 (Mifepristone)	Sigma-Aldrich	Cat# M8046
IM33	This paper	
Dihydroethidium	Sigma-Aldrich	Cat# 37291
Lipoic acid	Sigma-Aldrich	Cat# T5625
THIP (Gaboxadol hydrochloride)	Sigma-Aldrich	Cat# T101
Ampicillin	Sigma-Aldrich	Cat# A9518
Doxycycline	Sigma-Aldrich	Cat# D9891
Kanamycin	Sigma-Aldrich	Cat# B5264
Peptidoglycan	Sigma-Aldrich	Cat# 69554
Papain	Worthington Biochemical	LK003178
Collagenase I	Sigma-Aldrich	Cat# C2674
SYTOX green	Thermo Fisher Scientific	Cat# R37168
Critical commercial assays		
DNeasy blood and tissue kit	Qiagen	Cat# 69506
BCA protein assay kit	Fisher Scientific	Cat# 23225
Glucose (HK) Assay Kit	Sigma-Aldrich	GAHK20–1KT
Triglyceride Reagent	Sigma-Aldrich	T2449
DeadEnd fluorometric TUNEL system	Fisher Scientific	Cat# G3250
Mouse SLPI ELISA kit	LifeSpan Biosciences	LS-F6729–1
All-In-One 5X RT MasterMix	ABM	Cat# G592
Deposited data		
16S sequencing	This paper	BioProject PRJNA912676
Single-cell RNA sequencing	This paper	GSE185369
Experimental models: Cell lines		
Human: Expi293F Cells	Thermo Fisher Scientific	Cat# A14528

REAGENT or RESOURCE	SOURCE	IDENTIFIER
Experimental models: Organisms/strains		
Mouse: C57BL/6J	The Jackson Laboratory	RRID:IMSR_JAX:000664
D. melanogaster: y[1] v[1]; P{y[+t7.7] v[+t1.8]=UAS-LUC.VALIUM10}attP2	BDSC	RRID:BDSC_35788
D. melanogaster: y[1] v[1]; P{y[+t7.7] v[+t1.8]=TRiP.GL01213}attP40	BDSC	RRID:BDSC_41631
D. melanogaster: y[1] v[1]; P{y[+t7.7] v[+t1.8]=TRiP.HMS04250}attP2	BDSC	RRID:BDSC_56047
D. melanogaster: y[1] w[*]; P{w[+m*]=nSyb-GAL4.S}3	BDSC	RRID:BDSC_51635
D. melanogaster: w[1118]; P{w[+m*]=GAL4}repo/TM3, Sb[1]	BDSC	RRID:BDSC_7415
D. melanogaster: w[1118]	BDSC	RRID:BDSC_5905
D. melanogaster: y[1] w[*]; P{w[+mC]=Act5C-GAL4}25FO1/CyO, y[+]	BDSC	RRID:BDSC_4414
D. melanogaster: w[1118]; P{w[+mC]=UAS-RedStinger}6	BDSC	RRID:BDSC_8547
D. melanogaster: y[1] M{RFP[3xP3.PB] GFP[E.3xP3]=vas-Cas9}ZH-2A w[1118]/FM7c	BDSC	RRID:BDSC_51323
D. melanogaster: w[*]; P{w[+mC]=ppl-GAL4.P}2	BDSC	RRID:BDSC_58768
D. melanogaster: w[1118]; P{w[+mC]=Hml-GAL4.Delta}2	BDSC	RRID:BDSC_30139
D. melanogaster: w[*]; P{w[+mW.hs]=GawB}NP5130/CyO; P{w[+mC]=UAS-GC3Ai}3	BDSC	RRID:BDSC_84303
D. melanogaster: w[*]; P{w[+mW.hs]=GawB}Myo31DF[NP0001]; P{w[+mC]=UAS-GC3Ai}3	BDSC	RRID:BDSC_84307
D. melanogaster: IM33-GFP knock-in	This paper	
D. melanogaster: IM33 knockout	This paper	
D. melanogaster: UAS-IM33	This paper	
D. melanogaster: UAS-IM33-HA	This paper	
D. melanogaster: UAS-IM33$^{\Delta SP}$-HA	This paper	
D. melanogaster: IM33-Gal4	This paper	
D. melanogaster: w[*]; P{w[+mW.hs]=Switch2}GSG7293–1/TM6B, Tb[1]	BDSC	RRID:BDSC_59929
D. melanogaster: w[1118]; P{w[+mC]=UAS-GFP.nls}14	BDSC	RRID:BDSC_4775
D. melanogaster: w[*]; P{y[+t7.7] w[+mC]=10XUAS-mCD8::GFP}attP2	BDSC	RRID:BDSC_32184
D. melanogaster: w[1118]; P{y[+t7.7] w[+mC]=GMR23E10-lexA}attP40	BDSC	RRID:BDSC_52693
D. melanogaster: w[*]; P{w[+mC]=Ilp2-GAL4.R}2/CyO	BDSC	RRID:BDSC_37516
D. melanogaster: w[1118]; P{w[+mC]=Dh44-GAL4.TH}2M	BDSC	RRID:BDSC_51987
D. melanogaster: P{w[+mC]=Pdf-GAL4.P2.4}X, y[1] w[*]	BDSC	RRID:BDSC_6899
D. melanogaster: w[*]; TI{2A-GAL4}NPF[2A-GAL4]/TM6B, Tb[1]	BDSC	RRID:BDSC_84671
D. melanogaster: TI{2A-GAL4}ple[2A-GAL4]	BDSC	RRID:BDSC_86289
D. melanogaster: TI{2A-GAL4}ChAT[2A-GAL4]/TM3, Sb[1]	BDSC	RRID:BDSC_84618

REAGENT or RESOURCE	SOURCE	IDENTIFIER
D. melanogaster: w[*]; P{w[+mC]=LexAop-CD8-GFP-2A-CD8-GFP}2; P{w[+mC]=UAS-mLexA-VP16-NFAT}H2, P{w[+mC]=lexAop-rCD2-GFP}3/TM6B, Tb[1]	BDSC	RRID:BDSC_66542
D. melanogaster: w[1118]; PBac{y[+mDint2] w[+mC]=20XUAS-IVS-jGCaMP7c}VK00005	BDSC	RRID:BDSC_79030
D. melanogaster: y[1] sc[*] v[1] sev[21]; P{y[+t7.7] v[+t1.8]=TRiP.HMC06337}attP40	BDSC	RRID:BDSC_67236
D. melanogaster: y[1] sc[*] v[1] sev[21]; P{y[+t7.7] v[+t1.8]=TRiP.HMS00259}attP2	BDSC	RRID:BDSC_33383
D. melanogaster: y[1] sc[*] v[1] sev[21]; P{y[+t7.7] v[+t1.8]=TRiP.HMC05031}attP40	BDSC	RRID:BDSC_60038
D. melanogaster: y[1] v[1]; P{y[+t7.7] v[+t1.8]=TRiP.HMJ22903}attP40/CyO	BDSC	RRID:BDSC_60904
Oligonucleotides		
Primers used in this study: see Table S3	This paper	
Software and algorithms		
Fiji	http://fiji.sc	RRID:SCR_002285
RStudio	https://posit.co/	RStudio (RRID:SCR_000432)
GraphPad Prism	http://www.graphpad.com/	GraphPad Prism (RRID:SCR_002798)
Sleep analysis code	This paper	
ShinyR-DAM	Cichewicz, K. and J. Hirsh [53]	https://karolcichewicz.shinyapps.io/shinyr-dam/
DADA2	https://benjjneb.github.io/dada2/	DADA2 (RRID:SCR_023519)
Vegan	http://cran.r-project.org/web/packages/vegan/index.html	vegan (RRID:SCR_011950)
Phyloseq	http://www.bioconductor.org/packages/2.12/bioc/html/phyloseq.html	phyloseq (RRID:SCR_013080)
MaAsLin2	https://bioconductor.org/packages/release/bioc/html/Maaslin2.html	MaAsLin2 (RRID:SCR_023241)
10x Genomics Cellranger DNA	https://support.10xgenomics.com/single-cell-dna/software/pipelines/latest/what-is-cell-ranger-dna	10x Genomics Cellranger DNA (RRID:SCR_023221)
Seurat	https://satijalab.org/seurat/get_started.html	Seurat (RRID:SCR_016341)
clusterProfiler	http://bioconductor.org/packages/release/bioc/html/clusterProfiler.html	clusterProfiler (RRID:SCR_016884)